Brenden A. Magill, Kyoung-Duck Park, Yuan Zhou, Anuj Chopra, Deepam Maurya, Shashank Priya, Markus Raschke, Alexey Belyanin, Christopher J. Stanton and Giti A. Khodaparast*

Ultrafast Anisotropic Optical Response and Coherent Acoustic Phonon Generation in Polycrystalline BaTiO$_3$-BiFeO$_3$

Abstract: We optically study the as-yet little explored multiferroic material, BaTiO$_3$-BiFeO$_3$ (BTO-BFO), that has demonstrated enhanced magnetic properties, a higher DC resistance in comparison to BFO, and improved magnetoelectric coupling. Our studies include: ultrafast time resolved differential reflection, optically induced birefringence, and second-harmonic nano-imaging of the ferroic order. We observe a strong sensitivity to pump/probe polarizations, photo-induced ferroelectric poling on a picosecond timescale, as well as the generation of photo-induced coherent acoustic phonons with a frequency of ∼11 GHz. The second-harmonic generation nano-imaging reveals disordered but distinct ferroelectric domain order, percolating even across grain boundaries in the poly-crystalline thin film.

Keywords: Multiferroics, Time Resolved Spectroscopy, Second Harmonic Generation, Acoustic Phonons

1 Introduction

Multiferroic materials can exhibit simultaneous ferroelectric, ferromagnetic, and ferroelastic order (Eerenstein, Mathur, and Scott 2006, Zhao et al. 2006). They have been proposed for the conversion of light at optical frequencies into THz frequencies (Rana et al. 2009), DC polarizations (Yang et al. 2009), and for the fabrication of multifunctional devices

*Corresponding author: Giti A. Khodaparast, Department of Physics, Virginia Tech., Blacksburg, VA, USA

Brenden A. Magill, Department of Physics, Virginia Tech., Blacksburg, VA, USA

Kyoung-Duck Park, Department of Physics, Department of Chemistry, and JILA, University of Colorado Boulder, Boulder, CO, USA

Yuan Zhou, Anuj Chopra, Deepam Maurya, Shashank Priya, Department of Mechanical Engineering, Virgina Tech., Blacksburg, VA, USA

Markus Raschke, Department of Physics, Department of Chemistry, and JILA, University of Colorado Boulder, Boulder, CO, USA

Alexey Belyanin, Department of Physics & Astronomy, Texas A&M University, College Station, TX, USA

Christopher J. Stanton, Department of Physics, University of Florida, Gainesville, FL, USA

(Eerenstein, Mathur, and Scott 2006, Cheong and Mostovoy 2007, Ramesh and Spaldin 2007). BiFeO$_3$ (BFO) is a single phase multiferroic and has attracted a lot of interest due to its high Néel and Curie temperatures, as well as its ferroelectric and anti-ferromagnetic properties (Ederer and Spaldin 2005, Hur et al. 2004, Ryu et al. 2011). In BFO based systems, optically induced birefringence (Rivera and Schmid 1997), optically induced strain waves (Lejman et al. 2014, Chen et al. 2012), and electrical control of acoustic phonons (Rovillain et al. 2010) have been observed.

One inherent challenge in utilizing BFO for multifunction devices is that the large leakage currents, due to increased conductivity from oxygen vacancies and Fe ions, degrade its ferroelectric properties. In this paper we focus on a solid-state solution of BaTiO$_3$-BiFeO$_3$ (BTO-BFO) where the addition of another perovskite material reduces the conductivity of the composite material (Park et al. 2010, Yang et al. 2013). In addition, previous investigations on the BTO-BFO solid solutions have found the presence of a morphotropic phase boundary (MPB) (Yang et al. 2013). Further, this solid-state solution was an enhanced magnetoelectric properties for mole fraction between 72.5 %–75 % BFO with the 72.5 % BFO samples showing the strongest magneto-electric coupling. In these samples the enhancement of magnetic properties were attributed to active spin modulation of ordered Fe-O-Fe bond (Park et al. 2010, Yang et al. 2013). It was found that the substitution of large Ba^{2+} and Ti^{4+} ions on the A- and B- sites respectively enlarges the distortion of bond angle of Fe-O-Fe to release the spiral magnetic modulation. The atomic pair distribution function (PDF) for pure BFO ($x = 1.0$) was found to fit with a rhombohedral structure model (Space Group: R3c) with lattice parameters in hexagonal setting (a = 5.583 Å, c = 13.835 Å, and gamma = 120°). The PDFs for $(1-x)$BTO$-(x)$BFO ($x = 0.725$) were found to fit at lower r values with a structural model featuring monoclinic structure (Space Group: Cm) with parameters (a = 5.499Å, b = 5.631Å, c = 3.974Å, and beta = 91°). As the annealing temperature was varied between 700–900 °C, the XRD intensity of the perovskite peaks corresponding to (100), (110), and (111) was found to increase but there was no notable preferred orientation. At higher r values, a rhombohedral model (Space

Group: R3c) (a = 5.558Å, c = 13.834Å, and gamma = 120°) provided better fit. Thus, this material was found to be rhombohedral on average with local monoclinic distortions/symmetry. These results point towards the realization of a room temperature single phase multiferroic magnetoelectric material (Yang et al. 2013).

In this work, we report time resolved and second harmonic generation (SHG) measurements of (1–x)BTO–(x)BFO (x = 0.725), a multiferroic material with improved magnetoelectric properties. Our studies include ultrafast time resolved differential reflection (TRDR), time resolved optically induced birefringence (TROIB), time resolved Magneto-Optical Kerr Effect (MOKE), and SHG nano-imaging to study the underlying domain order. We observe a high sensitivity to pump/probe polarizations, disordered but distinct ferroelectric order percolating even across grain boundaries in the poly-crystalline thin film, photo-induced ferroelectric poling on a picosecond timescale, and the generation photo-induced strain pulses. The optical studies presented in this paper build upon of our prior structural analysis (Park et al. 2010, Yang et al. 2013). The BTO-BFO has a ferroelectric Curie temperature of ~1103 K and an anti-ferromagnetic Néel temperature of ~643 K. Since BTO-BFO is a solid state mixture, it exists in a single phase rather than in separate components; therefore, our observed response is a combined effect of the whole solution. Our X-ray measurements (Magill et al. 2015) reveals that the film is in pure perovskite phase.
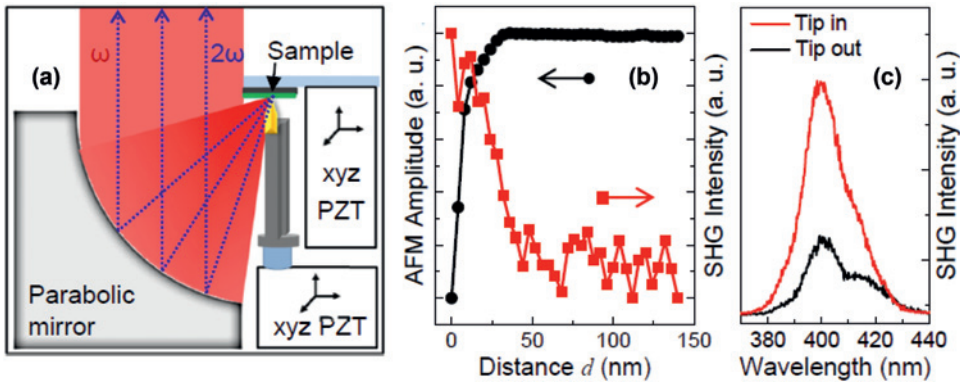
2 Experimental Approach

For our optical measurements we used a Ti:Sapphire amplifier with repetition rate of 1kHz, center wavelength of 800 nm, and pulse duration of 100 fs. The laser pulses were split into a pump and a probe beam. The pump pulses were delayed using a moving mirror, then frequency doubled to 400 nm via a 0.5 mm thick BBO crystal. The pump and probe beams were focused and overlapped on the sample at an angle of 45°. The probe beam has a spot size of 150 – 200 μm with the pump being slightly larger. The time evolution of the reflectivity was measured to extract the pump-induced change in carrier dynamics. For our TROIB measurements, the polarization of the pump and probe pulses were set via half wave plates. In the TROIB measurements, the reflected light travels through a Wollaston prism to separate the S and P polarizations of the reflected pulses. Balanced photodiode detection was used to measure the differences between the S and P polarizations as a function of the time delay between the pump and probe pulses. A similar setup was used for the MOKE (Kini et al. 2008) measurements with the pump pulses being circularly polarized.

In order to relate the macroscopic measurements that average over multiple domains to the underlying microscopic domain order, we use the symmetry selectivity of SHG both in far-field, and for near-field nano-imaging, in scattering scanning near-field optical microscopy (s-SNOM) geometry, to determine symmetry characteristics and the ferroelectric (FE) domain texture of the BTO-BFO films as described previously (Neacsu et al. 2009, Atkin et al. 2012). Figure 1(a) shows the schematic of the experiment, based on a combination of a parabolic mirror based excitation and detection scheme (Sackrow et al. 2008), with axial illumination and detection and a shear-force AFM based near-field SHG imaging implementation (Neacsu et al. 2009). Pump radiation provided from a Ti: sapphire oscillator (Femtolasers Inc., with $\tau \cong 11$ fs pulse duration and 78 MHz repetition rate, power < 8 mW) is focused onto the scanning probe gold tip, with polarization controlled by a half-wave plate. The tip-enhanced and backscattered SHG signals are polarization selected, filtered using dichroic optics, and detected using a spectrometer with a LN_2 cooled charge-coupled device (CCD). Specific combinations of input and output polarizations and the predominant enhancement of the tip-parallel polarization allow one to select specific nonlinear susceptibility components, characteristic to the ferroelectric domains, and their orientation (Atkin et al. 2012; Neacsu et al. 2009). Figure 1(b)–(c) shows spatial and spectral characteristics of the near-field SHG signal.

3 Results and Discussions

The poly-crystalline BTO-BFO for this study is composed of a mixture of BTO and BFO and was grown on platinized (100) silicon substrate using KrF excimer pulsed laser (λ = 248 nm) deposition (PLD). A stoichiometric 0.275BTO–0.725BFO target was synthesized by conventional mixed-oxide processing route (Park et al. 2010; Yang et al. 2013). The sample for cross-sectional transmission electron microscopy (TEM) was prepared by standard focused ion beam etching technique. Figure 2 shows a cross-sectional TEM image of the sample, consists of island structures that are irregularly distributed in the films with an average size of ~100 nm and a 40 nm thick flat region between them. This suggests that the BTO-BFO films are growing in Volmer-Weber growth mode possibly because the cohesive energy of the atoms within the film is greater than that between the film and substrate resulting in island formation (Esat, Bell, and Comyn 2014). The typical atomic % between Bi/Fe for island region was calculated to be 1.91 which is almost 10 times higher than that in the flat region.

Figure 1: (a) Schematic of the experimental setup for SHG nano-imaging. (b) Approach curve of Au tip to the BTO-BFO surface with near-field increase of SHG intensity in shear force regime. (c) Near- and far-field SHG spectra.
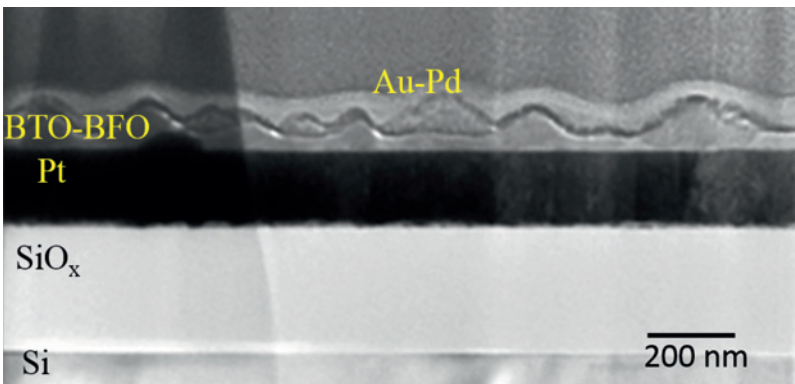

Figure 2: Cross sectional TEM (Jeol 4010 at 200 V) of the BTO-BFO film with Si substrate, and the Pt wetting layer. An Au-Pd layer was deposited on top of the BTO-BFO to facilitate focused ion beam extraction.

For TRDR measurements, we employed a two color technique, with the pump wavelength of 400 nm (3.09 eV) between the bandgaps of BFO (2.67 eV) (Xu et al. 2009) and BTO (3.50 eV) (Joshi and Desu 1997; An et al. 2011; Jin et al. 2012), where our optical absorption measurements demonstrated a large absorption at 400 nm, and the probe wavelength of 800 nm (1.55 eV) below both bandgaps. In Figure 3, we show examples of the TRDR, where the difference between the pump and the probe polarizations are 0°, 30°, 60°, and 90° (where 0° refers to the pump and probe polarizations being parallel), as shown in the inset of Figure 3. These pump-probe transients display a sharp initial decrease in the reflectivity, followed by a fast recovery over 2 ps, and finally a slower relaxation towards zero. This observation was consistent over all the probed spots, suggesting that the local disorder in the poly-crystalline film is not playing an important role, even in the presence of long range anisotropy in this film.

The fits to ΔR/R are described by a double exponential function with slow and fast components. From these fits, several time scales can be extracted: a fast decay (2–7 ps)

and a slower time scale, on the order of a few hundreds of ps. Single scattering events such as electron-phonon scattering or hot electron thermalization (i. e., the electrons relaxing through electron-electron scattering) typically occur on a less than 200 fs time scales, so this is too fast for the 2–7 ps time scale process. Hence we find that the ~2–7 ps decay component is not due to a simple, single scattering process. Instead, the initial 2–7 ps time decay could correspond to an intermediate time-scale scattering process which involves several scattering events. The materials system studied here are complicated and as a result, it is difficult to know exactly what are these carrier scattering processes. In semiconductors such as GaAs, (Stanton and Bailey 1992) one sees 2–10 ps change in the time-dependent differential reflectivity similar to that shown here. This relaxation time is associated with the scattering of electrons via the electron-phonon interaction out of the central Γ valley into the satellite L valleys then back into the central Γ valley (Bailey, Stanton, and Hess 1990). The reflectivity is dominated by the number of electrons in the lightest mass valley (Γ) and the time dependence comes from the slow
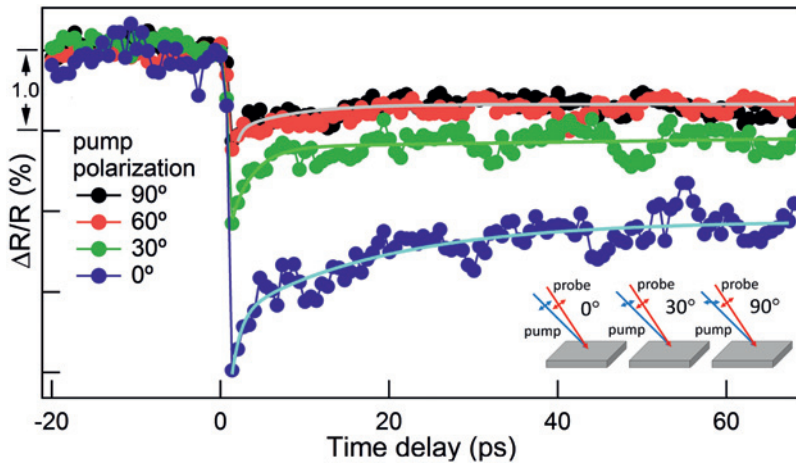
Figure 3: TRDR of BTO-BFO at 300 K, with the pump fluence of 3.80 mJ cm^{-2}, and the ratio of the pump to probe energy 1000:1. Dotted lines are the experimental data while the solid lines are the double exponential fits. The time scale for the fast relaxation decreases as the polarization angle is increased (from 7.1 ps at 0° to 2.6 ps at 30°) while the time constant for the slow relaxation indicates slow components of 334 ps at 0° to 765 ps at 30. The inset presents linear rotations of the 0°, 30°, and 90° to the pump pulse polarization while the polarization of the probe pulses is held constant.

return of the electron back in to the Γ valley. It is not clear whether a similar process can occur in the BFO-BTO system since the detailed band structure of the system is lacking. It is possible, that this 2–7 ps rise of the differential reflectivity, results from carriers which thermalize to the bottom of the conduction band (and also possibly the top of the valence band). This can lead to a time-dependent (dynamic) Burstein-Moss shift which changes the absorption edge (Ulman et al. 1993) and can additionally lead to a change in the index of refraction and hence a change in the differential reflectivity.

Although the probe frequency is sub-bandgap, the change in reflectivity is still due to the complex refractive index associated with interband transitions. Excitation and subsequent phonon-mediated energy relaxation of carriers changes the occupation of electron and hole states which leads to fast variation of the complex refractive index. Another possible "intermediate time" scattering mechanism can originate from the diffusion of the photoexcited carriers (for 400 nm pulses, the absorption length in this material is about 32 nm) across the film thickness where they can recombine due to defects at the interface. In BFO, the photo-excited carriers are expected to have a relatively long lifetime (1–2 ns) (Sheu et al. 2012), which could not be detected in the range of our experimental setup. In addition, time-resolved synchrotron x-ray diffraction measurements in BFO, demonstrated that the strain developed within 100 ps, relaxed in several ns (Wen et al. 2013).

For longer time scales, as shown in Figure 4, there is also a sinusoidal oscillation in the TRDR. The black line in Figure 4 is the sinusoidal fit to the observed oscillation and has a frequency of ∼11 GHz (we refer to the frequency as $\omega = 2\pi f$). We attribute the observed oscillation to the generation of photo-induced coherent acoustic phonons in the BTO-BFO. The period of the strain pulse is determined by the sound velocity of the transverse acoustic (TA) modes which is determined by the relevant bulk modulus of the material. Similar oscillations have been observed in BFO and have been ascribed to coherent acoustic phonons in the BFO (Chen et al. 2012; Lejman et al. 2014). Our observed frequency of ∼11 GHz is within the range of frequencies for transverse
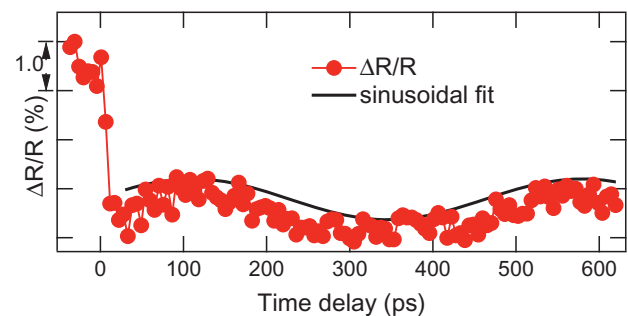
**Figure 4:** TRDR measurement of the BTO-BFO at room temperature for a pump fluence of 1.92 mJ cm^{-2} and a pump/probe ratio of 5000:1. here, the pump and probe polarizations are perpendicular to each other.

coherent acoustic phonons observed in BFO (Lejman et al. 2014). This TA mode was detected with no detectable sign of the longitudinal acoustic phonons (LA). In most of metals and semiconductors, the magnitudes of TA phonons are usually much smaller that of the simultaneously generated LA phonons, which could be a disadvantage for applications (Lejman et al. 2014). These acoustic phonons then modulate the refractive index which disturbs the optical reflectivity of the sample and is measured by the probe beam through the acousto-optic effect. In our experiment, this corresponds to a sinusoidal modulation of the optical reflectivity $\Delta R/R$ in the time domain as shown in Figure 4.

Using 800 nm with the absorption length of $\sim 1\ \mu m$ allowed us to probe the observed dynamics deeply beneath the BFO-BTO layer. We could still get a clear signal of acoustic phonons because of the favorable combination of above-band gap pump and below-gap probe (Lejman et al. 2014; Ruello et al. 2012). The energy of the incoming pump pulses with 100-fs duration is instantaneously deposited in the BFO-BTO film over an area (150–200 μm pump beam diameter) much larger than the film thickness, creating a coherent acoustic wave with a plane phase front. The below-gap 800 nm probe reflects off the whole excitation volume creating a strong oscillating signal in TRDR.

We also explored the transient birefringence by probing the changes in the polarization of the reflected probe pulses ($\Delta\theta$), as a function of the time delay. Figure 5 shows the time evolution of the transient birefringence for different pump/probe polarization angles. At the zero time delay, we observed an initial sharp increase in θ, followed by a fast relaxation over ~ 10 ps and then a slower dynamic in $\Delta\theta$ that eventually results in the sign change of θ, remaining negative over the rest of the temporal range of our setup (1.2 ns). Moreover, the sign change occurs after 600–800 ps so it is most likely due to much slower processes than the changes in carrier distribution, for example dynamics of the electric polarization, resulting from photoexcited carrier recombination and lattice vibrations. The cross over of the signal at which the sign of $\Delta\theta$ changes from the positive to negative, occurs at shorter time delays (as shown by the arrows in Figure 5), as the pump polarization is varied towards increasing polarization angle between the pump and probe. The magnitude of the increase in $\Delta\theta$ is independent of the pump polarization.

The decay of $\Delta\theta$ also displays exponential behavior and can be fit to a double exponential consisting of fast and slow components. Both time scales decrease as the relative pump/probe polarization angle is increased. The fast decay time, decreases from 23.6 ps at 0°, to 6.6 ps at 90°. Similarly the slow component's time scale decreases as the polarization
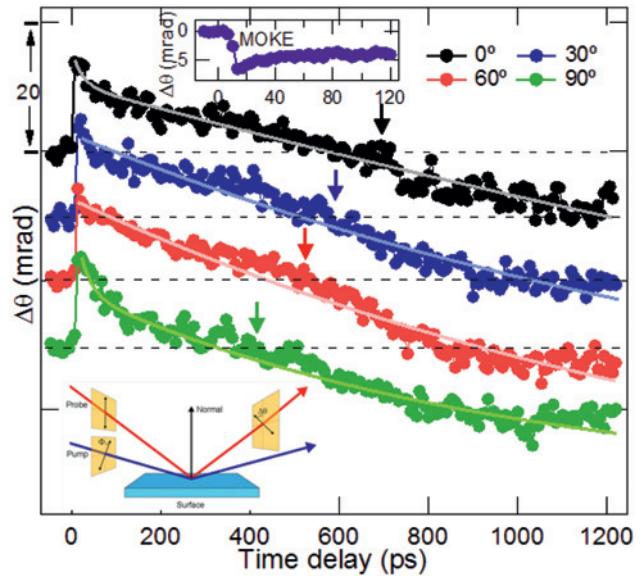
Figure 5: TROIB of the BTO-BFO at room temperature with 800 nm probe and 400 nm pump, a pump fluence of 3.40 mJ cm^{-2} with four different linear polarization between the pump and probe pulses. Traces are offset by -10 mrad for clarity. Inset: time resolved MOKE measurement. The cartoon: We define the linear polarization angle of the pump, Φ and the $\Delta\theta$ which is the rotation of the probe polarization after reflection off the sample. In our measurements, the polarization angle of the probe pulse is fixed in the plane of incidence, so Φ is the angle of the pump polarization with respect to the polarization of the probe pulses, and to the plane of incidence.

angle of the pump is increased, changing from 603 ps at 0° to 229 ps at 90° (when the fits end where the sign changes). As shown in the inset of Figure 5 unlike the transient birefringence, the photo-induced time-resolved MOKE (Kini et al. 2008) does not change sign. In multi-layer structures, MOKE in general is a mixture of "absorptive" (resonant) and "dispersive" contributions, so that the response has a component related to the average magneto-optical activity which in turn is some weighted average of spin polarization over the bands and can result in a different dynamics compared to TROIB (Zak et al. 1990, 1991).

Our SHG results both in near- and far-field, demonstrate similar sensitivity to polarization, as observed in our TRDR and TROIB measurements. Figure 6(a) shows a far-field rotational SHG anisotropy detected in the reflection mode with P- and S-polarized excitation (P_{in} and S_{in}), and indicates a significant net sample ferroelectric polarization (offset angle due to arbitrary sample orientation with respect to incident polarization). The S_{in} SHG signal is larger than for P_{in} due to the loss of in-plane electric field component due to the angle of incidence. The finite signal is the result of incomplete domain cancelation due to the small laser focus, angle of incidence, and
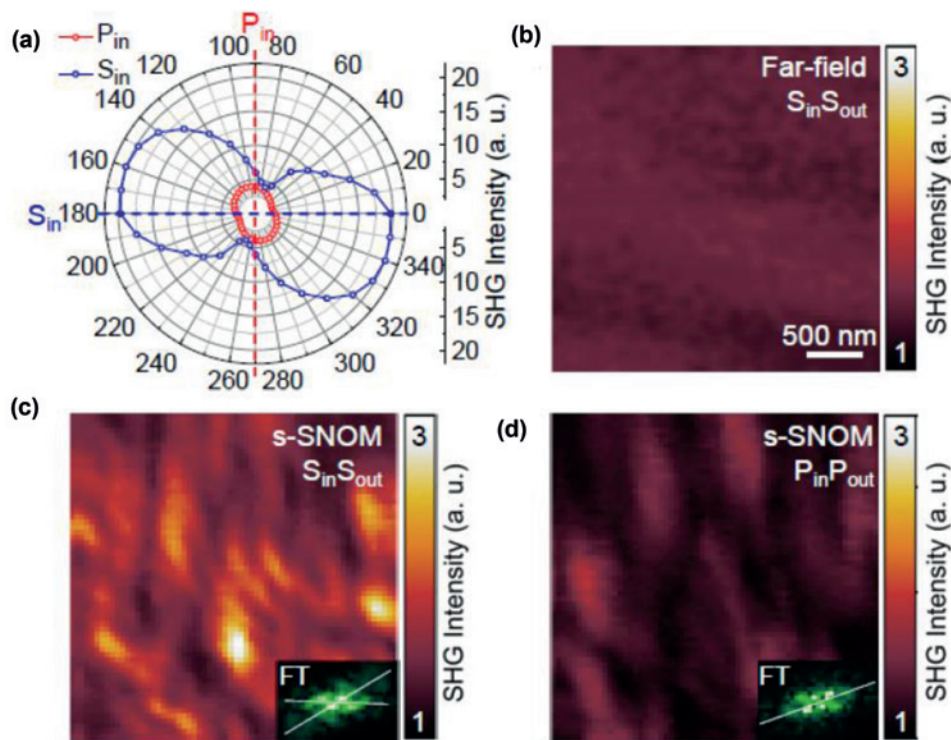
Figure 6: (a) Far-field SHG polar plots of BTO-BFO for P_{in} and S_{in} excitations. (b) Far-field SHG image for $S_{in}S_{out}$ polarization selection. Near-field SHG images for $S_{in}S_{out}$ (c) and $P_{in}P_{out}$ (d) polarization exhibiting disordered, but generally typical, complex FE domain order. Inset: 2D image Fourier transform, indicating the primary domain orientations.

retardation effects. However, no specific domain contrast is observed in the far-field SHG response (Figure 6(b)). It is also of note, that we do not observe the presence of any magnon side bands which have been previously observed in BFO (Ramirez et al. 2009). On the other hand, distinct ferroelectric (FE) domain contrast is observed in near-field SHG imaging (Figure 6(c) and (d)) under both $S_{in}S_{out}$ and $P_{in}P_{out}$ polarization combination as a superposition of amplitude and heterodyne phase contrast SHG due to interference with the far-field SHG background, as described previously (Neacsu et al. 2009; Atkin et al. 2012). Despite the polycrystalline film structure, distinct FE contrast is observed with domains extending over multiple crystallites. The FE domains are highly disordered but otherwise exhibit predominantly two ($S_{in}S_{out}$), or one ($P_{in}P_{out}$) dominant orientations, as also seen in the 2D Fourier transformed image (inset). These FE features are generally observed over extended sample regions. The spatial features are similar to the complex domain structures of BFO thin films and other multiferroics systems as observed previously by TEM and piezo-response force microscopy (PFM) (Zhao et al. 2006). Furthermore, both the generation of far field SHG and the magnitude of the TROIB response are sensitive to the polarization of

the pump pulses suggesting a link between these two phenomena. The transient nature of the TROIB response combined with our observations of large ferroelectric domains in the nano-SHG cause us to attribute this response to optically driven poling in the BTO-BFO.

In summary, we report time-resolved and SHG measurements of $(1-x)$BTO-(x)BFO $(x = 0.725)$. Our results showed the sensitivity of TROIB to the difference in the linear polarization of the pump and probe pulses. In concert with the near and far field SHG emissions, we conclude that the optical rectification originating from photo-induced electrical polarization in our film could be the main mechanism for the strain. This clear sensitivity of the poling in the polycrystalline film to the polarization of the incident light and the observation of FE domains, larger than the individual grains in the film, suggests that there are non-local orders, despite disordered surface displayed in the TEM image. The reduced symmetry of this morphology, in comparison to a film, could be the origin of both the strong anisotropy with respect to polarization and the strong SHG response. Our time resolved optically induced strain and electrical polarization suggest that BTO-BFO could be used for applications translating GHz and THz optical signals

into acoustic or electrical signals (Takahashi, Kida, and Tonouchi 2006; Rana et al. 2009; Pradarutti et al. 2007; Kim and Gopalan 2001; Hong et al. 2008; Akimov et al. 2006; Moss et al. 2011), for use in electro-optical modulation of waveguides similar to BFO (Li et al. 2013), to manipulate magnetism in composite multiferroic ferromagnetic devices (Davis, Baruth, and Adenwalla 2010), and spin manipulation over short time scales in ferromagnetic materials (Sterbinsky et al. 2010).

References

Akimov, A. V., A. V. Scherbakov, D. R. Yakovlev, C. T. Foxon, and M. Bayer. 2006. "Ultrafast Band-Gap Shift Induced by a Strain Pulse in Semiconductor Heterostructures." *Physical Review Letters* 97:037401.

An, Y. Q., A. J. Taylor, S. D. Conradson, S. A. Trugman, T. Durakiewicz, and G. Rodriguez. 2011. "Ultrafast Hopping Dynamics of 5F Electrons in the Mott Insulator UO_2 Studied by Femtosecond Pump-Probe Spectroscopy." *Physical Review Letters* 106:207402.

Atkin, J. M., S. Berweger, A. C. Jones, and M. B. Raschke. 2012. "Nano-Optical Imaging and Spectroscopy of Order, Phases, and Domains in Complex Solids." *Advances in Physics* 61:745–842.

Bailey, D. W., C. J. Stanton, and K. Hess. 1990. "Numerical Studies of Femtosecond Carrier Dynamics in GaAs." *Physical Review B* 42:3423–34.

Chen, L. Y., J. C. Yang, C. W. Luo, C. W. Laing, K. H. Wu, J. -Y. Lin, T. M. Uen, J. Y. Juang, Y. H. Chu, and T. Kobayashi. 2012. "Ultrafast Photoinduced Mechanical Strain in Epitaxial $BiFeO_3$ Thin Films." *Applied Physics Letters* 101:041902.

Cheong, S. -W., and M. Mostovoy. 2007. "Multiferroics: A Magnetic Twist for Ferroelectricity." *Nature Materials* 6:13–20.

Davis, S., A. Baruth, and S. Adenwalla. 2010. "Magnetization Dynamics Triggered by Surface Acoustic Waves." *Applied Physics Letters* 97:232507.

Ederer, C., and N. A. Spaldin. 2005. "Weak Ferromagnetism and Magnetoelectric Coupling in Bismuth Ferrite." *Physical Review B* 71:060401.

Eerenstein, W., N. D. Mathur, and J. F. Scott. 2006. "Multiferroic and Magnetoelectric Materials." *Nature* 442:759–65.

Esat, F., A. J. Bell, and T. P. Comyn. 2014. "Microstructure development of $BiFeO_3$-$PbTiO_3$ films deposited by pulsed laser deposition on platinum substrates." *Acta Materialia* 66:44–53.

Hong, K. -H., J. Kim, S. -H. Lee, and J. K. Shin. 2008. "Strain-Driven Electronic Band Structure Modulation of Si Nanowires." *Nano Letters* 8:1335–40.

Hur, N., S. Park, P. A. Sharma, J. S. Ahn, S. Guha, and S. W. Cheong. 2004. "Electric Polarization Reversal and Memory in a Multiferroic Material Induced by Magnetic Fields." *Nature* 429:392–5.

Jin, Z., Y. Xu, Z. Zhang, G. Li, X. Lin, G. Ma, Z. Cheng, and X. Wang. 2012. "Structural Dependent Ultrafast Electron-Phonon Coupling in Multiferroic $BiFeO_3$ Films." *Applied Physics Letters* 100:071105.

Joshi, P., and S. Desu. 1997. "Structural, Electrical, and Optical Studies on Rapid Thermally Processed Ferroelectric $BaTiO_3$ Thin Films Prepared by Metallo-Organic Solution Deposition Technique." *Thin Solid Films* 300:289–94.

Kim, S., and V. Gopalan. 2001. "Strain-Tunable Photonic Band Gap Crystals." *Applied Physics Letters* 78:3015–17.

Kini, R. N., K. Nontapot, G. A. Khodaparast, R. E. Welser, and L. J. Guido. 2008. "Time Resolved Measurements of Spin and Carrier Dynamics in InAs Films." *Journal of Applied Physics* 103:064318.

Lejman, M., G. Vaudel, I. C. Infante, P. Gemeiner, V. E. Gusev, B. Dkhil, and P. Ruello. 2014. "Giant Ultrafast Photo-Induced Shear Strain in Ferroelectric $BiFeO_3$." *Nature Communications* 5:1–7.

Li, J., Z. Liu, Y. Tu, S. -T. Ho, I. W. Jung, L. Ocola, and B. Wessels. 2013. "Photonic Crystal Waveguide Electro-Optic Modulator with a Wide Bandwidth." *Journal of Light-Wave Technology* 31:1601–7.

Magill, B. A., M. Bishop, S. A. McGill, Y. Zhou, A. Chopra, D. Maurya, H. -C. Song, S. Priya, and G. A. Khodaparast. 2015. "Ultrafast Magneto-Optical Spectroscopy of $BiFeO_3$-$BaTiO_3$ Based Structures." *Proc. of SPIE* 9551:95510T.

Moss, D. M., A. V. Akimov, B. A. Glavin, M. Henini, and A. J. Kent. 2011. "Ultrafast Strain-Induced Current in a GaAs Schottky Diode." *Physical Review Letters* 106:066602.

Neacsu, C. C., B. B. van Aken, M. Fiebig, and M. B. Raschke. 2009. "Second-Harmonic Near-Field Imaging of Ferroelectric Domain Structure of $YMnO_3$." *Physical Review B* 79:100107.

Park, T. -J., G. C. Papaefthymiou, A. J. Viescas, Y. Lee, H. Zhou, and S. S. Wong. 2010. "Composition-Dependent Magnetic Properties of $BiFeO_3$-$BaTiO_3$ Solid Solution Nanostructures." *Physical Review B* 82:024431.

Pradarutti, B., G. Matthus, S. Riehemann, G. Notni, J. Limpert, S. Nolte, and A. Tnnermann. 2007. "Electro-Optical Sampling of Ultrashort THz Pulses by fs-Laser Pulses at 530 Nm with $BaTiO_3$." *Journal of Applied Physics* 102:093105.

Ramesh, R., and N. A. Spaldin. 2007. "Multiferroics: Progress and Prospects in Thin Films." *Nature Materials* 6:21–9.

Ramirez, M. O., A. Kumar, S. A. Denev, N. J. Podraza, X. S. Xu, R. C. Rai, Y. H. Chu, J. Seidel, L. W. Martin, S. -Y. Yang, et al. 2009. "Magnon Sidebands and Spin-Charge Coupling in Bismuth Ferrite Probed by Nonlinear Optical Spectroscopy." *Physical Review B* 79:224106.

Rana, D. S., I. Kawayama, K. Mavani, K. Takahashi, H. Murakami, and M. Tonouchi. 2009. "Understanding the Nature of Ultrafast Polarization Dynamics of Ferroelectric Memory in the Multiferroic $BiFeO_3$." *Advanced Materials* 21:2881–5.

Rivera, J. P., and H. Schmid. 1997. "On the Birefringence of Magnetoelectric $BiFeO_3$." *Ferroelectrics* 204:23–33.

Rovillain, P., R. de Sousa, Y. Gallais, A. Sacuto, M. A. Masson, D. Colson, A. Forget, M. Bibes, A. Barthlmy, and M. Cazayous. 2010. "Electric-Field Control of Spin Waves at Room Temperature in Multiferroic $BiFeO_3$." *Nature Materials* 9:975–9.

Ruello, P., T. Pezeril, S. Avanesyan, G. Vaudel, V. Gusev, I. C. Infante, and B. Dkhil. 2012. "Photoexcitation of Gigahertz Longitudinal and Shear Acoustic Waves in $BiFeO_3$ Multiferroic Single Crystal." *Applied Physics Letters* 100:212906.

Ryu, J., C. -W. Baek, Y. -S. Lee, N. -K. Oh, G. Han, J. -W. Kim, B. -D. Hahn, J. -J. Choi, W. -H. Yoon, J. -H. Choi, et al. 2011. "Enhancement of Multiferroic Properties in $BiFeO_3$-Ba$(Cu_{1/3}Nb_{2/3})O_3$: Film Fabricated by Aerosol Deposition." *Journal of the American Ceramic Society* 94:355–8.

Sackrow, M., C. Stanciu, M. A. Lieb, and A. J. Meixner. 2008. "Imaging Nanometre-Sized Hot Spots on Smooth Au Films with High-Resolution Tip-Enhanced Luminescence and Raman Near-Field Optical Microscopy." *ChemPhysChem* 9:316–20.

Sheu, Y. M., S. A. Trugman, Y. -S. Park, S. Lee, H. T. Yi, S. -W. Cheong, Q. X. Jia, A. J. Taylor, and R. P. Prasankumar. 2012. "Ultrafast Carrier Dynamics and Radiative Recombination in Multiferroic $BiFeO_3$." *Applied Physics Letters* 100:242904.

Stanton, C. J., and D. W. Bailey. 1992. "Rate Equations for the Study of Femtosecond Intervalley Scattering in Compound Semiconductors." *Physical Review B* 45:8369–77.

Sterbinsky, G. E., B. W. Wessels, J. -W. Kim, E. Karapetrova, P. J. Ryan, and D. J. Keavney. 2010. "Strain-Driven Spin Reorientation in Magnetite/Barium Titanate Heterostructures." *Applied Physics Letters* 96:092510.

Takahashi, K., N. Kida, and M. Tonouchi. 2006. "Terahertz Radiation by an Ultrafast Spontaneous Polarization Modulation of Multiferroic $BiFeO_3$ Thin Films." *Physical Review Letters* 96:117402.

Ulman, M., D. W. Bailey, L. H. Acioli, F. G. Vallée, C. J. Stanton, E. P. Ippen, and J. G. Fujimoto. 1993. "Femtosecond Tunable Nonlinear Absorption Spectroscopy in $Al_{0.1}Ga_{0.9}$As." *Physical Review B* 47:10267–78.

Wen, H., P. Chen, M. P. Cosgriff, D. A. Walko, J. H. Lee, C. Adamo, R. D. Schaller, J. F. Ihlefeld, E. M. Dufresne, D. G. Schlom, et al. 2013. "Electronic Origin of Ultrafast Photoinduced Strain in $BiFeO_3$." *Physical Review Letters* 110:037601.

Xu, X. S., T. V. Brinzari, S. Lee, Y. H. Chu, L. W. Martin, A. Kumar, S. McGill, R. C. Rai, R. Ramesh, V. Gopalan, et al. 2009. "Optical Properties and Magnetochromism in Multiferroic $BiFeO_3$." *Physical Review B* 79:134425.

Yang, S. -C., A. Kumar, V. Petkov, and S. Priya. 2013. "Room-Temperature Magnetoelectric Coupling in Single-Phase $BaTiO_3$-$BiFeO_3$ System." *Journal of Applied Physics* 113:144101.

Yang, S. Y., L. W. Martin, S. J. Byrnes, T. E. Conry, S. R. Basu, D. Paran, L. Reichertz, J. Ihlefeld, C. Adamo, A. Melville, et al. 2009. "Photovoltaic Effects in $BiFeO_3$." *Applied Physics Letters* 95.

Zak, J., E. R. Moog, C. Liu, and S. D. Bader. 1990. "Fundamental magneto-optics." *Journal of Applied Physics* 68:4203.

Zak, J., E. R. Moog, C. Liu, and S. D. Bader. 1991. "Magneto-optics of multilayers with arbitrary magnetization directions." *Physical Review B* 43:6243.

Zhao, T., A. Scholl, F. Zavaliche, K. Lee, M. Barry, A. Doran, M. P. Cruz, Y. H. Chu, C. Ederer, N. A. Spaldin, et al. 2006. "Electrical Control of Antiferromagnetic Domains in Multiferroic $BiFeO_3$ Films at Room Temperature." *Nature Materials* 5:823–9.